Journal of Power Sources 183 (2008) 118–125

Contents lists available at ScienceDirect

Journal of Power Sources

journal homepage: www.elsevier.com/locate/jpowsour

Electrochemical parameter estimation in operating proton exchange membrane fuel cells

M.A. Rubio[a,*], A. Urquia[a], R. Kuhn[b], S. Dormido[a]

[a] Departamento de Informática y Automática, UNED, Juan del Rosal 16, 28040 Madrid, Spain
[b] Centre for Solar Energy and Hydrogen Research (ZSW), Ulm, Germany

ARTICLE INFO

Article history:
Received 26 February 2008
Received in revised form 10 April 2008
Accepted 4 May 2008
Available online 9 May 2008

Keywords:
Diagnosis
Impedance spectroscopy
Identification
Electrochemical parameters
Flooding

ABSTRACT

A novel methodology for the diagnosis of an operating proton exchange membrane fuel cell (PEMFC) is proposed in this manuscript. The cell impedance can be represented as the sum of two terms: the membrane resistance and a second-order transfer function. An experimental procedure and a method to estimate the parameters of this impedance model from the experimental data, by applying parameter identification techniques, are proposed. The experimental procedure consists in reading the dynamic response of the cell voltage and current after the occurrence of small changes in the load value. This experimental procedure, intended for application on operating cells, does not significantly interfere with the cell operation. It has been designed supposing that the frequency range of the relevant cell phenomena is 1 Hz to 5 kHz. The required experimental equipment is inexpensive and easily portable. Analytical relationships have been derived in order to calculate the following cell electrochemical parameters from the model parameters: the diffusion resistance, the charge transfer resistance, the diffusion-related time constant, the membrane resistance and the double layer capacitance.

1. Introduction

Our society is suffering from fossil fuel shortage. Fossil fuels (i.e., coal, oil, and natural gas) also contribute to a number of environmental problems during their extraction, transportation, and use. As an alternative for the devices consuming fossil fuels, fuel cells are one of the most promising means of producing energy in portable systems. In particular, the use of proton exchange membrane fuel cells (PEMFCs) in automotive systems is a very active and promising research field. Fuel cell vehicles offer substantial reductions in greenhouse gas emissions [1] and higher energy efficiency than internal combustion engine vehicles [2].

Mathematical models have been proposed in order to understand the physical and chemical phenomena involved in the PEMFC operation. These include 1D [3–6], 2D [7] and 3D [8,9] static models; and 1D [10,11], and 3D [12] dynamic models. The water flooding in the PEMFC cathode has been modeled from physical–chemical first principles [13]. These detailed models contain a large number of adjustable parameters and their computation time is large.

PEMFC models with low computational cost, intended for use in control applications, have also been developed. In this context, Randles electric models and electrical impedance spectroscopy (EIS) techniques are employed to study the fuel cell behavior and to estimate the value of the cell model parameters [14–22]. However, EIS equipment is too expensive [23] and bulky for use on continuous in-field assessment of operating portable PEMFC systems. Therefore, this approach to PEMFC diagnosis is not suited for in-field control applications, which require of easily portable and inexpensive diagnosis equipment, able to be integrated into the portable power systems.

Parameter estimation techniques have been successfully applied by other authors. An ARX model was proposed in [24] for describing the dynamic response of solid oxide fuel cells. Other approach to PEMFC modeling was proposed in [25]: the dynamic response of the PEMFC is represented by a transfer function matrix whose inputs are the cell current and the oxygen stoichiometry. The use of ARMAX models, with the oxygen and hydrogen flows as model inputs, and PRBS signals was proposed in [26]. However, these approaches neither provides a procedure for estimating the cell physical–chemical parameters from the cell model, nor relates the estimated transfer function and the cell impedance.

A method for diagnosis of PEMFC through current interruption (CI), intended to be used in portable control systems, was proposed in [27]. It exhibits the following advantages [27]: the equipment required to make the measurements is easily portable and inexpensive, the proposed cell equivalent-circuit model has

* Corresponding author. Tel.: +34 913987147; fax: +34 91 398 7690.
E-mail addresses: marubio@dia.uned.es (M.A. Rubio), aurquia@dia.uned.es (A. Urquia), robert.kuhn@zsw-bw.de (R. Kuhn), sdormido@dia.uned.es (S. Dormido).

0378-7753/$ – see front matter © 2008 Elsevier B.V. All rights reserved.
doi:10.1016/j.jpowsour.2008.05.011

Nomenclature

C_{dl}	double layer capacitance (F)
C_g	concentration in cathode active layer (mol m^{-3})
D	diffusion coefficient (m^2 s^{-1})
E_{oc}	open circuit voltage (V)
f	Faraday constant (F)
N	cycle length (bit)
R	perfect gas constant (J mol^{-1} K^{-1})
R_d	diffusion resistance (Ω)
R_m	membrane resistance (Ω)
R_p	charge transfer resistance (Ω)
s	Laplace transform variable
S	active area (m^2)
T	temperature (K)
T_{sw}	inverse of the signal rate (s bit^{-1})
Z_W	Warburg impedance

Greek letters

α	signal amplitude (V)
δ	diffusion layer thickness (m)
η_a	anode over-voltage (V)
η_c	cathode over-voltage (V)
η_m	membrane over-voltage (V)
τ_d	diffusion-related time constant (s)
ω	frequency (rad s^{-1})

low computational cost, and the PEMFC electrochemical parameters can be calculated from the model parameters. However, this diagnosis method exhibits the following limitation. As the data acquisition method for parameter estimation requires to completely interrupt the cell current, this cell diagnosis method interferes with the cell operation.

The main objective of the work presented in this manuscript is to propose a cell diagnosis methodology with all the advantages of the method proposed in [27] and without the disadvantage of interfering with the cell operation.

A simplification of the PEMFC model presented in [27] is proposed in this manuscript. In addition, an experimental procedure and a method to estimate the parameters of this simplified model from the experimental data, by applying parameter identification techniques, are proposed. The data acquisition procedure, which can be applied during the cell operation, consists in reading the change in the cell voltage and current induced by small changes in the load resistance. Analytical relationships have been derived in order to calculate the cell electrochemical parameters from the simplified model parameters. The proposed diagnosis methodology allows precise estimation of the following cell electrochemical parameters: the diffusion resistance, the charge transfer resistance, the diffusion-related time constant and the membrane resistance. The model simplification is obtained at the cost of increasing the error in the estimation of the double layer capacitance, whose value is underestimated. A numeric fitting function of the error made in the estimation of the double layer capacitance is provided. This expression allows correcting the value of the double layer capacitance, reducing significantly the estimation error.

2. Experimental set-up and procedure

The modelling and parametric identification of the PEMFC impedance will be addressed in Section 3. In particular, the cell impedance is represented by Eq. (1), and a procedure is proposed for estimating the parameters R_m, b, c, e and f from the cell experimental data.

$$Z_{cell}(s) = R_m + \frac{bs + c}{es^2 + fs + 1} \quad (1)$$

The acquisition of the experimental data is discussed in this section. Essentially, it consists in reading the dynamic response of the cell voltage and current after the occurrence of small changes in the load value. This experimental procedure, intended for application on operating cells, does not significantly interfere with the cell operation.

2.1. Experimental set-up

The characteristics of the PEMFC used in the study are 100 cm^2 electrode surface; GORE 5761 membrane with membrane thickness 19 μm; SGL 10 BB material used as GDL; and serpentine flow-field at the anode and the cathode side. The operating conditions are the cell temperature is not controlled during the experiment; the PEMFC is fed with air and hydrogen at atmospheric pressure; the hydrogen flow is 0.05 ml min^{-1}; and three air flows are used: 0.61 ml min^{-1}, 0.51 ml min^{-1} and 0.32 ml min^{-1}. The EIS measurements are made using a IM6 (ZAHNER electrik) workstation.

The PEMFC, the load and the circuit intended to produce small changes in the load value are schematically represented in Fig. 1 a. The PEMFC equivalent circuit is the subcircuit named 'FC'. The load resistance is R_L. It sets the cell operating point. A resistor R_l (with $R_l \gg R_L$) and a switch represent the circuit added to perform the experimental tests. It allows forcing small changes in the load value, which produce small excursions from the cell operating point.

An implementation of this test bench is shown in Fig. 1b. The switch is implemented using a N-MOSFET, whose gate-to-source voltage is set by a signal generator. As the N-MOSFET channel resistance can be controlled by manipulating the gate-to-source voltage, in some cases the resistor R_l does not need to be included in the circuit.

A microcontroller with digital output is used to generate the N-MOSFET gate-to-source voltage (see Fig. 1b). The voltage waveforms used during the identification process are rectangular pulse-trains and pseudo-random binary sequences (PRBSs). The PRBS signals are generated by using a shift register [28]. The reasons behind the selection of this voltage signals will be discussed in Sections 3.4 and 3.5.

The analyzer device can be designed to perform the parametric identification calculations described in Section 3.6. Recursive least squares estimation, widely used in adaptive control [26,29], can be used. Nevertheless, the results discussed in this manuscript have been obtained by using off-line identification, which requires storing the signals in the memory of the analyzer device.

2.2. Experimental procedure

The following two considerations have been taken into account when designing the experimental procedure. The value of the drain current, while the N-MOSFET is in the on-state, needs to be small enough to justify the linear approximation, while maintaining an acceptable signal-to-noise ratio. The changes in the cell voltage induced by the load changes should be smaller than the thermal voltage (i.e., approximately 26 mV at 300 K) [30].

The data acquisition procedure consists of the following three steps:

(1) Firstly, a 5-kHz rectangular pulse-train with a 50% duty cycle is applied to the N-MOSFET gate for 80 ms. The cell voltage and current is read with a sampling period of 10 μs. This data is

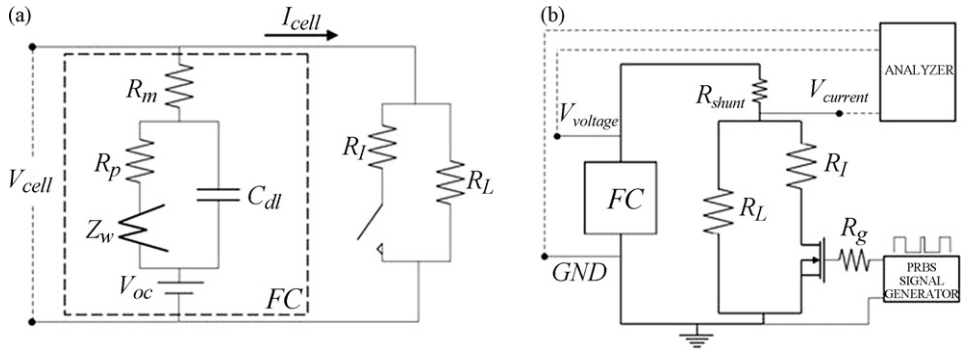

Fig. 1. Experimental set-up: (a) schematic representation and (b) implementation using an N-MOSFET device.

used to estimate the value of the membrane resistance (R_m). The procedure is discussed in Section 3.4.

(2) Next, the high-frequency PRBS voltage waveform described in Table 1 is applied to the N-MOSFET gate for 0.15 s. The cell voltage and current is read with a sampling period of 10 μs.

(3) Finally, the low-frequency PRBS voltage waveform described in Table 1 is applied to the N-MOSFET gate for 13 s. The cell voltage and current is read with a sampling period of 500 μs.

The data obtained from Steps (2) and (3) is used to estimate the parameters *b*, *c*, *e* and *f*, by applying the parametric identification techniques described in Section 3.6.

3. Analysis and modeling

3.1. Main assumptions

The voltage drop across the fuel cell (V_{cell}) can be written as a function of the steady-state open-circuit voltage of the cell (E_{oc}), and the over-voltages of the anode (η_a), the cathode (η_c) and the membrane (η_m) [31,32]:

$$V_{cell} = E_{oc} - \eta_a - \eta_m - \eta_c \quad (2)$$

The open-circuit voltage (E_{oc}) is modeled as an ideal voltage source. The external operating conditions and the cell current are considered constant during the experiments. Therefore, the over-voltages (η_a, η_m, η_c) are assumed to be only dependent on the FC internal phenomena. The over-voltages of the different layers can be modeled as electric components that represent the FC dynamic behavior.

The cell voltage in Eq. (2) can be modeled by the electric circuit shown in Fig. 2a, which is composed of Randles models connected in series [15,33]. Z_W^a and Z_W^c are the Warburg impedances associated to the gas diffusion in the anode and the cathode, respectively. R_p^a and R_p^c are the charge transfer resistances in the anode and the cathode. C_{dl}^a and C_{dl}^c are the double layer capacities in the anode and the cathode. Finally, R_m is the membrane resistance.

Two additional hypotheses are made in order to simplify the cell model shown in Fig. 2a. As a result, the simplified model shown in Fig. 2b is obtained.

(1) The oxygen reduction reaction in the cathode is very slow in comparison with the hydrogen oxidation reaction [34,35]. Therefore, the anode over-voltage is very small in comparison with the cathode over-voltage. As a consequence, the anode over-voltage contribution to the cell voltage can be neglected in the model.

(2) The double layer capacity, which is usually represented by constant-phase elements, is represented by a pure, single-frequency theoretical capacity [16,22,33,36]. This approximation, which reduces the computational cost of the model, is reasonably accurate at low and medium frequencies (i.e., frequencies below a few hundred Hz). The error due to this hypothesis is justified for the sake of obtaining a model simple enough to be suited for control applications.

3.2. Modelling of the Warburg impedance

The Warburg impedance (Z_W) can be written in the Laplace domain as a function of the finite length diffusion [15]:

$$Z_W(s) = R_d \frac{\tanh\sqrt{s\tau_d}}{\sqrt{s\tau_d}} \quad (3)$$

where the diffusion resistance (R_d) and the diffusion time constant (τ_d) can be calculated from the following expressions:

$$R_d = \frac{RT\delta}{SC_g Dn^2F^2} \quad (4)$$

$$\tau_d = \frac{\delta^2}{D} \quad (5)$$

The approximation of the Warburg impedance shown in Eq. (6) was proposed in [27]. This approximation is equivalent to model the cell by using the circuit shown in Fig. 3. The value of the parameters R_1, R_2, C_1 and C_2 were calculated in [27] and they are shown in Table 2.

$$Z_W(s) = R_d\left(\frac{R_1}{1+R_1C_1\tau_d s} + \frac{R_2}{1+R_2C_2\tau_d s}\right) \quad (6)$$

The exact value of the impedance, calculated from Eq. (3), and the approximated value, obtained from Eq. (6) using the previously calculated values of R_1, R_2, C_1 and C_2, are plotted in Fig. 4. The absolute error is also shown in Fig. 4. Frequencies (ω) in the range from 1 rad s^{-1} to 10^4 rad s^{-1} and diffusion-related time constants (τ_d) in

Table 1
Parameters defining the two PRBS voltage waveforms applied during the data acquisition process

	Low-frequency PRBS	High-frequency PRBS
Frequency range (Hz)	0.77–75	71–2 × 10^3
Cycle length (*N*, bit)	217	63
Period (T_{sw}, s bit^{-1})	5.94 × 10^{-3}	2.23 × 10^{-4}
Number of cycles	10	10

Table 2
Fitted values of the parameters in Eq. (6)

Parameter	Value	Units
R_1	0.8463	Unitless
R_2	0.1033	Unitless
C_1	0.3550	Unitless
C_2	0.03145	Unitless

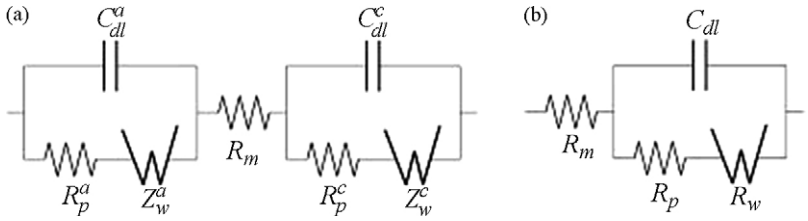

Fig. 2. Equivalent circuit models of the PEMFC: (a) complete model and (b) simplified model.

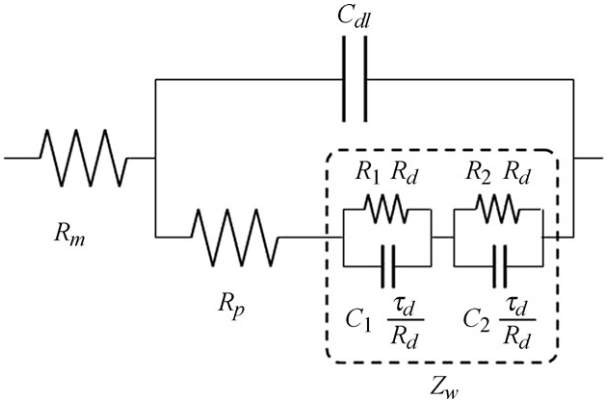

Fig. 3. Equivalent circuit model of the PEMFC with the Warburg impedance calculated from Eq. (6).

the range from 0.2 s to 1 s have been considered. As a consequence, the range of $jw\tau_d$ in Fig. 4 is 0.2 to 10^4.

3.3. Modelling of the PEMFC impedance

The cell impedance (Z_{cell}), calculated from the circuit shown in Fig. 3, is as follows:

$$Z_{cell}(s) = R_m + \frac{1}{sC_{dl} + (1/R_p + Z_W)} \quad (7)$$

It can be written as follows:

$$Z_{cell}(s) = R_m + \frac{as^2 + bs + c}{ds^3 + es^2 + fs + g} \quad (8)$$

where the parameters a, b, c, d, e and f are related to the cell electrochemical parameters as shown below [27].

$$a = 9.76 \times 10^{-4} R_p \tau_d^2 \quad (9)$$

$$b = 0.304 R_p \tau_d + 3.38 \times 10^{-2} R_d \tau_d \quad (10)$$

$$c = R_p + 0.949 R_d \quad (11)$$

$$d = 9.76 \times 10^{-4} C_{dl} R_p \tau_d^2 \quad (12)$$

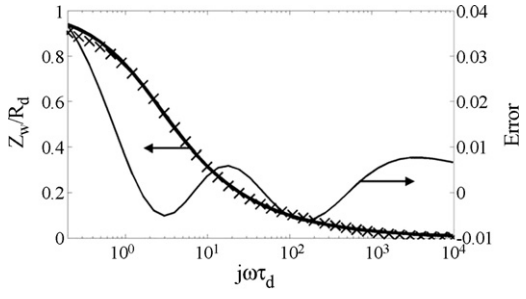

Fig. 4. Warburg impedance calculated from Eq. (3)(−) and Eq. (6)(×). Absolute error.

$$e = 3.37 \times 10^{-2} C_{dl} R_d \tau_d + 0.3048 C_{dl} R_p \tau_d + 9.76 \times 10^{-4} \tau_d^2 \quad (13)$$

$$f = C_{dl} R_p + 0.3048 \tau_d + 0.949 C_{dl} R_d \quad (14)$$

$$g = 1 \quad (15)$$

A further approximation for the cell impedance is proposed in this manuscript, which reduces the order of the model and, consequently, its computation time. The parameters a and d, which are two orders of magnitude smaller than the other parameters (i.e., b, c, e, f and g), are neglected in Eq. (8). Making this approximation, the following model for the cell impedance is obtained:

$$Z_{cell}(s) = R_m + \frac{bs + c}{es^2 + fs + 1} \quad (16)$$

Once the parameters b, c, e and f have been estimated from the cell experimental data, the following cell electrochemical parameters can be calculated from Eqs. (10), (11), (13) and (14): the double layer capacitance (C_{dl}), the diffusion resistance (R_d), the charge transfer resistance (R_p) and the diffusion-related time constant (τ_d).

The models described by Eqs. (8) and (16) predict the same steady-state value of the cell impedance:

$$\lim_{s \to 0}[Z_{cell}(s)] = R_m + c = R_m + R_p + 0.949 R_d \quad (17)$$

This value of the steady-state impedance can be calculated directly from the circuit shown in Fig. 3, by replacing the capacitors by open-circuits. As $R_1 = 0.8463$ and $R_2 = 0.1033$ [27], the value obtained by adding R_1 and R_2 is 0.949.

The proposed simplification of the impedance model does not introduce additional error in the estimation of the diffusion resistance (R_d), the charge transfer resistance (R_p) and the diffusion-related time constant (τ_d). The model simplification is made at the cost of increasing the error in the estimation of the double layer capacitance (C_{dl}), whose value is underestimated.

The error in the estimation of the double layer capacitance ($\varepsilon_{C_{dl}}$) is approximately described by Eq. (18). Therefore, the double layer capacitance is estimated by adding the following two terms: (a) the value calculated from the estimated model parameters (i.e., b, c, e and f) using Eqs. (10), (11), (13) and (14) and (b) the estimation error calculated from the following equation:

$$\varepsilon_{C_{dl}} = -0.005155 R_p^{-0.9197} \tau_d - 0.2629 R_d \tau_d + 0.02855 \tau_d \quad (18)$$

3.4. Estimation of the membrane resistance

As it was described in Section 2.2, the experimental data required to estimate the membrane resistance (R_m) is obtained by applying a 5 kHz rectangular pulse-train voltage to the N-MOSFET gate for 80 ms. The cell current and voltage are read with a sampling period of 10 μs.

The R_m term in Eq. (16) constitutes a proportionality factor between the changes in the cell current and voltage. The effect of the membrane resistance manifests at high frequencies, usually overlapping with the high-frequency inductive behavior, which is

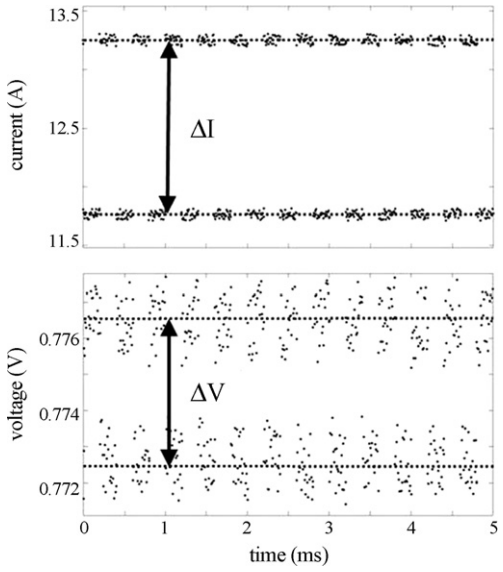

Fig. 5. Simulated change in the cell current (ΔI) and voltage (ΔV) in response to the applied N-MOSFET gate-to-source voltage (i.e., 5 kHz pulse-train with 50% duty cycle). The membrane resistance is $R_m \simeq \frac{|\Delta V|}{|\Delta I|}$.

represented by Z_i in Eq. (19). The method used to estimate the membrane resistance is described by Eq. (20). An example is shown in Fig. 5.

$$\lim_{s\to\infty} Z_{cell}(s) = R_m + Z_i(s) \tag{19}$$

$$\mathrm{Re}\left[\lim_{s\to\infty} Z_{cell}(s)\right] = R_m \simeq \frac{|\Delta V|}{|\Delta I|} \tag{20}$$

3.5. Selection of the PRBS voltage signals

In order to estimate the parameters b, c, e and f in Eq. (16), two PRBS voltage waveforms are applied to the N-MOSFET gate (see Section 2.2). The reason for using two PRBS signals instead of only one PRBS signal is reducing the number of collected experimental samples. In order to justify this assertion, the use of only one PRBS voltage waveform is considered first.

The frequency range for the relevant cell phenomena is supposed to be 1 Hz to 2 kHz. On the other hand, the spectral power of a PRBS signal generated using an shift register is described by Eq. (21)[28]. The signal frequency range, $[\omega_{inf}, \omega_{sup}]$, is shown in Eq. (22), where N is the cycle length, T_{sw} is the inverse of the signal rate and α is the signal amplitude.

$$\Phi(\omega) = \frac{\alpha^2(N+1)T_{sw}}{N}\left[\frac{\sin(\omega T_{sw})}{\omega T_{sw}/2}\right]^2 \tag{21}$$

$$\omega_{inf} = \frac{2\pi}{T_{sw}N} \le \omega \le \frac{2.8}{T_{sw}} = \omega_{sup} \tag{22}$$

Once the desired frequency range has been selected (i.e., the values of ω_{inf} and ω_{sup} have been set), the corresponding values of T_{sw} and N can be calculated from Eq. (22). In order to cover the frequency range of the cell relevant phenomena (i.e., 1 Hz to 2 kHz), the frequency range of the PRBS waveform should be $[\omega_{inf} = 2\pi, \omega_{sup} = 4\pi 10^3]\mathrm{rad\,s^{-1}}$.

While the PRBS voltage waveforms are applied to the N-MOSFET gate, the cell voltage and current need to be read with a sampling frequency of at least 10 times T_{sw}. As a consequence, the sampling frequency needs to be at least $4.5 \times 10^4 \mathrm{samples\,s^{-1}}$. On the other hand, adopting the heuristic criterium of collecting data at least during 10 cycles of the PRBS voltage waveform, the data acquisition process takes at least $10T_{sw}N$. For this frequency range selection (i.e., $\omega_{inf} = 2\pi\,\mathrm{rad\,s^{-1}} \rightarrow T_{sw}N = 2\pi/\omega_{inf} = 1\mathrm{s\,cycle^{-1}}$), the process should take at least 10 s. Considering that the sampling frequency needs to be at least 4.5×10^4 samples $\mathrm{s^{-1}}$, the total number of samples should be at least 4.5×10^5 samples.

An alternative approach consists in first applying 10 cycles of a low-frequency PRBS signal, whose frequency range is 0.77–75 Hz, and next applying 10 cycles of a high-frequency PRBS signal, whose frequency range is 71 Hz to 2 kHz. The characteristics of these two waveforms are summarized in Table 1 and their frequency spectrum is shown in Fig. 6. This approach allows reducing the number of samples in an order of magnitude (i.e., the required number of samples is now approximately 4×10^4 samples). As a consequence, using only one PRBS signal to cover all the frequency range is impractical, because it leads to an unnecessarily large number of samples.

3.6. Estimation of the parameters b, c, e and f

The cell voltage and current measured during the application of the two PRBS voltage signals are used to estimate the impedance parameters b, c, e and f. As $Z_{cell}(s) = V_{cell}(s)/I_{cell}(s)$, the parametric identification is performed by considering that the cell current (I_{cell}) is the process input and the cell voltage (V_{cell}) is the process output.

The effect of the membrane resistance is substracted from the measured cell voltage (V_{cell}) as shown in Eq. (23). The cell current (I_{cell}) and the calculated cell voltage (V^*_{cell}) are used to estimate the parameters b, c, e and f on the basis of Eq. (24). To this end, the frequency domain system identification toolbox for Matlab, called *Ident*, has been used.

$$V^*_{cell} = V_{cell} - R_m I_{cell} \tag{23}$$

$$V^*_{cell}(s) = \frac{bs + c}{es^2 + fs + 1} I_{cell}(s) \tag{24}$$

The *Ident* toolbox for Matlab allows estimating the coefficients of the transfer function shown in the following equation:

$$V^*_{cell}(s) = \frac{k(1 + T_z s)}{(1 + T_{p1}s)(1 + T_{p2}s)} I_{cell}(s) \tag{25}$$

The parameters b, c, e and f can be calculated from the coefficients k, T_z, T_{p1}, T_{p2} using the following equations:

$$c = k \tag{26}$$

$$b = kT_z \tag{27}$$

$$e = T_{p1}T_{p2} \tag{28}$$

$$f = T_{p1} + T_{p2} \tag{29}$$

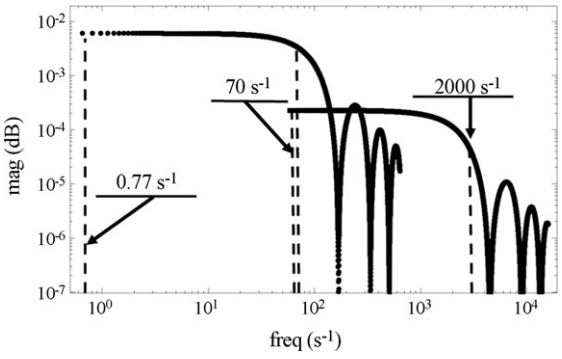

Fig. 6. Frequency spectrum of the two PRBS signals described in Table 1.

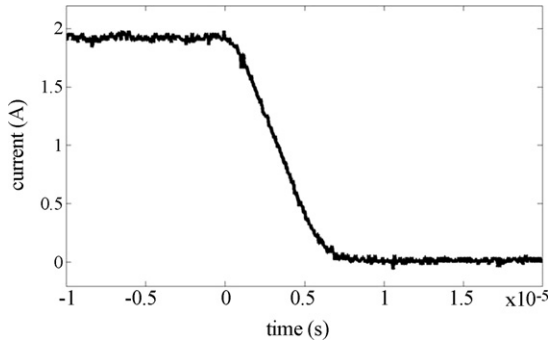

Fig. 7. Drain current of a IRFZ48 MOSFET connected to a single PEMFC as shown in Fig. 1b. Switching time is under 10^{-5} s.

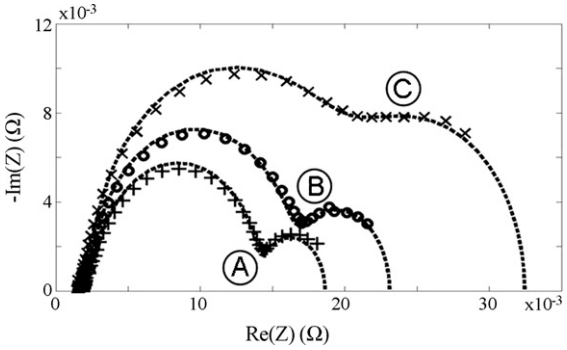

Fig. 9. EIS spectrum corresponding to the following air flows: (A) 0.61 ml min^{-1}, (B) 0.51 ml min^{-1} and (C) 0.32 ml min^{-1}; and fitted third-order models (- -).

Table 3
Cell parameters corresponding to successive stages in the cathode flooding process

Curve	C_{dl} (F)	R_d (mΩ)	R_p (mΩ)	τ_d (s)	R_m (mΩ)
A	0.253	5.769	10.6	0.751	2.562
B	0.372	7.969	13.2	0.698	2.343
C	0.587	12.69	18.1	0.409	2.304

4. Results and discussion

The test circuit shown in Fig. 1b allows obtaining switching times under 10^{-5} s. An example is shown in Fig. 7. As the time constant of the cell response is typically above 10^{-4} s, switching can be considered instantaneous.

The PRBS voltage applied to the N-MOSFET gate induces changes in the cell current whose waveform is not exactly a PRBS (see Fig. 8 a). Nevertheless, the cell current exhibits a frequency response similar to the frequency response of a PRBS (see Fig. 8b). PRBS changes in the cell current could be obtained by using galvanostatic equipment. However, the proposed procedure allows obtaining the desired result by using inexpensive and easy-to-use equipment.

In order to compare the results obtained from the third-order and the second-order impedance models, described by Eqs. (8) and (16), respectively, the following study has been performed.

EIS measurements have been made on the cell and under the experimental conditions described in Section 2.1. In order to induce different stages of the flooding process, three air flows have been used. The results are shown in Fig. 9. The third-order impedance model has been fitted to the experimental data corresponding to these flooding process stages, named A, B and C. The electrochemical parameters of the cell, calculated from the fitted models, are shown in Table 3.

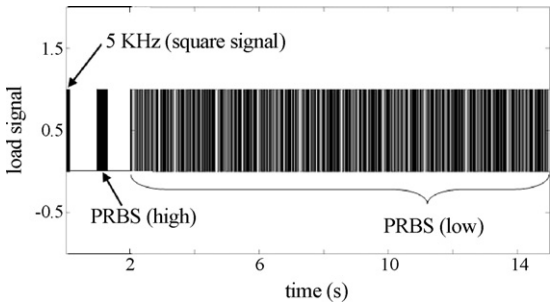

Fig. 10. State of the switch that controls the load changes during the data acquisition process (1: closed; 0: open).

Firstly, the data acquisition procedure and the cell voltage have been simulated at these three different stages of the cathode flooding process, using the third-order impedance model. The state of the switch that controls the load changes during the simulated experimental run is represented in Fig. 10. The pulse-train voltage waveform is applied to the N-MOSFET gate in the first place. Next, the two PRBS voltage waveforms are applied.

Secondly, uniformly distributed noise has been added to the cell voltage and current values obtained by simulating the experimental procedure. Each simulated value of the cell current has been incremented by a $U(-50, 50)$ mA distributed random variate. Analogously, each simulated cell voltage has been incremented by a $U(-1, 1)$ mV distributed random variate.

For instance, the cell voltage calculated from the third-order impedance model during the application of the low-frequency PRBS voltage, and modified by adding the corresponding $U(-1, 1)$ mV distributed random variate, is represented by dots in Fig. 11. The

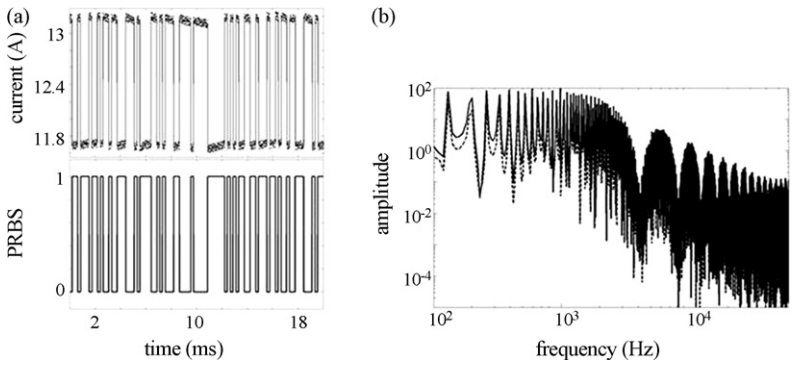

Fig. 8. Response to the high-frequency PRBS voltage waveform applied to the N-MOSFET gate: (a) cell current and applied voltage and (b) frequency spectrums of the cell current and the applied voltage.

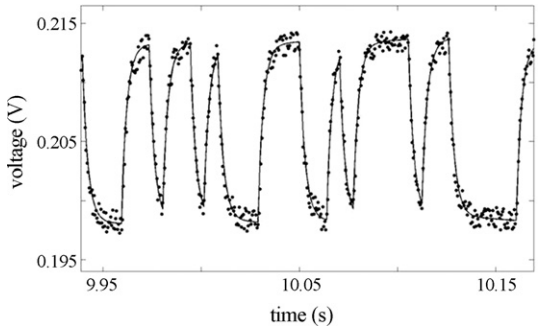

Fig. 11. Cell voltage during the application of the low-frequency PRBS voltage waveform. Simulated experimental data (dots) corresponding to the "A" flooding process stage and values predicted by using the fitted second-order impedance model (continuous line curve).

Table 4
Parameters estimated using the diagnosis method proposed in this manuscript

Curve	C_{dl} (F)	R_d (mΩ)	R_p (mΩ)	τ_d (s)	R_m (mΩ)
A	0.323	5.322	11.02	0.807	2.620
B	0.446	7.866	13.30	0.715	2.402
C	0.678	12.930	17.87	0.453	2.396

impedance model parameters correspond to the A stage of the cathode flooding process (see Table 3).

Thirdly, the cell voltage and current values previously calculated have been used to estimate the parameters of the second-order impedance model. Three impedance models are obtained, corresponding to the three flooding process stages. The Nyquist and Bode diagrams for the third-order and the second-order impedance models are shown in Fig. 12. Continuing with the example shown in Fig. 11, the corresponding cell voltage predicted by the second-order impedance model is represented by a continuous line curve in Fig. 11.

Finally, the cell electrochemical parameters predicted by the second-order impedance models are calculated. They are shown in Table 4. The values of the double layer capacitance have been corrected by adding the corresponding estimated errors, which are evaluated from Eq. (18).

Comparing the results shown in Tables 3 and 4, the conclusion is that the model simplification and the data acquisition procedure proposed in this manuscript do not introduce additional error in the estimation of the following electrochemical parameters: the membrane resistance (R_m), the diffusion resistance (R_d), the charge transfer resistance (R_p) and the diffusion-related time constant (τ_d). The impedance model simplification is made at the cost of increasing the error in the estimation of the double layer capacitance (C_{dl}), whose value is underestimated. A more precise estimation of the double layer capacitance is obtained by adding to the estimated value the correction term described by Eq. (18).

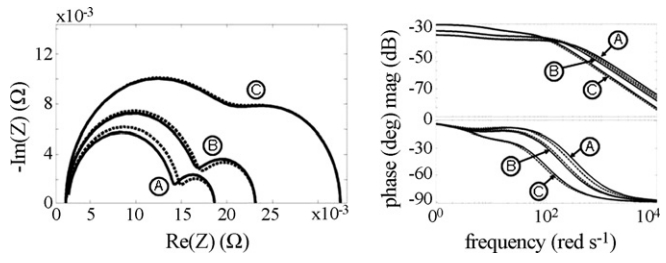

Fig. 12. Nyquist and Bode diagrams for the third-order (—) and the second-order (- -) impedance models, corresponding to three different flooding process stages.

5. Conclusions

A method for electrochemical parameter estimation in operating PEMFC has been discussed in this manuscript. It has the three main advantages of the method proposed in [27]. Firstly, the equipment required to make the experimental measurements is easily portable and inexpensive. Secondly, the proposed cell impedance model is well-suited for control applications: it has low computational cost and it allows reproducing the dynamic behavior of the PEMFC. Finally, the following PEMFC electrochemical parameters can be calculated from the model parameters: the diffusion resistance, the charge transfer resistance, the diffusion-related time constant, the membrane resistance and the double layer capacitance. The proposed diagnosis method has an additional advantage: the experimental measurements can be performed during the cell operation. The data acquisition procedure does not interfere with the cell operation. It consists in reading the change in the cell voltage and current induced by small changes in the load resistance.

Acknowledgments

This work has been supported by the Spanish CICYT, under DPI-2007-61068 grant, and by the IV PRICIT (Plan Regional de Ciencia y Tecnologia de la Comunidad de Madrid, 2005-2008), under S-0505/DPI/0391 grant.

The experimental work was developed in the Centre for Solar Energy and Hydrogen Research (ZSW), Ulm, Germany.

The authors are grateful to ZSW people, especially to Christoph Hartnig to coordinate the lab's work, Juergen Kaczerowski for the experimental setup and Joachim Scholta for his suggestions about the measurement system.

Finally, thanks to Michael Danzer, of the Ulm University, for his valuable discussions and feedback.

References

[1] M. Granovskii, I. Dincer, M.A. Rosen, Int. J. Hydrogen Energy 32 (8) (2006) 927–931.
[2] R.K. Ahluwalia, X. Wang, J. Power Sources 177 (2008) 167–176.
[3] D.M. Bernardi, M.W. Verbrugge, J. Electrochem. Soc. 139 (1992) 2477–2491.
[4] K. Broka, P. Ekdunge, J. Appl. Electrochem. (1997) 27.
[5] V. Gurau, H. Liu, S. Kakac, AIChE J. 44 (1998) 2410–2422.
[6] A. Rowe, X. Li, J. Power Sources 102 (2001) 82–96.
[7] J.S. Yi, T.V. Nguyen, J. Electrochem. Soc. 145 (1998) 1149–1159.
[8] S. Um, C.Y. Wang, J. Power Sources 125 (2004) 40–51.
[9] T. Zhou, H. Liu, J. Power Sources 138 (2004) 101–110.
[10] D. Bevers, M. Wöhr, K. Yasuda, K. Oguro, J. Appl. Electrochem. (1997) 27.
[11] M. Ceraolo, C. Miulli, A. Pozio, J. Power Sources 113 (2003) 131–144.
[12] B.R. Silversen, N. Djalali, J. Power Sources 141 (2005) 65–78.
[13] T.E. Springer, M.S. Wilson, J. Electrochem. Soc. 140 (1993) 3513–3526.
[14] T.E. Springer, Rainstrick, J. Electrochem. Soc. 136 (1989) 1594–1603.
[15] J.R. Macdonald, Impedance Spectroscopy, John Wiley & Sons, Canada, 1987.
[16] A.G. Hombrados, L. Gonzalez, M.A. Rubio, W. Agila, E. Villanueva, D. Guinea, E. Chimarro, D. Moreno, J.R. Jurado, J. Power Sources 151 (2005) 25–31.
[17] M. Boillot, C. Bonnet, N. Jatroudakis, P. Carre, S. Didierjean, F. Lapicque, Fuel Cells 1 (2006) 31–37.
[18] N. Wagner, J. Appl. Electrochem. 32 (2002) 859–863.
[19] M. Ciureanu, H. Wang, J. Electrochem. Soc. 146 (11) (1999) 4031–4040.
[20] B. Andreaus, A.J. McEvoy, G.G. Scherer, Electrochem. Acta 47 (2002) 2223–2229.
[21] X. Yuan, J.C. Sun, M. Blanco, H. Wang, J. Zhang, D.P. Wilkinson, J. Power Sources 161 (2006) 920–928.
[22] N. Fouquet, C. Doulet, C. Nouillant, G. Dauphin-Tauguy, B. Ould-Bouamama, J. Power Sources 159 (2005) 905–913.
[23] A. Carullo, F. Ferraris, M. Parvis, A. Vallan, E. Angelini, P. Spinelli, IEEE Trans. Instrum. Meas. 49 (2) (2000) 371–375.
[24] F. Jurado, J. Power Sources 129 (2004) 205–215.
[25] M. Buchholz, V. Krebs, Fuel Cells 7 (5) (2007) 392–401.
[26] Y.P. Yang, F.C. Wang, H.P. Chang, Y.-W. Ma, B.J. Weng, J. Power Sources 164 (2007) 761–771.

[27] M.A. Rubio, A. Urquia, S. Dormido, J. Power Sources 171 (2007) 670–677.
[28] M.W. Braun, D.E. Rivera, A. Stenman, W. Foslien, C. Hrenya, Proceedings of the American Control Conference, San Diego, 1999.
[29] L. Ljung, T. Söderström, Theory and Practice of Recursive Identification, MIT Press, 1987.
[30] Jer-Nan Juang, Applied System Identification, New Jersey, 1994.
[31] J. Larminie, A. Dicks, Fuel Cell System Explained, John Wiley & Sons, England, 2000.
[32] R.F. Mann, J.C. Amphlett, M.A.I. Hooper, H.M. Jensen, B.A. Peppley, P.R. Roberge, J. Power Sources 86 (2000) 173–180.
[33] M. Usman Iftikhar, D. Riu, F. Druart, S. Rosini, Y. Bultel, N. Retiere, J. Power Sources 160 (2006) 1170–1182.
[34] D. Natarajan, T.V. Nguyen, J. Electrochem. Soc. 148 (2001) 1324–1335.
[35] L. Pisani, G. Murgia, M. Valentini, B. D'Aguanno, J. Power Sources 108 (2002) 192–203.
[36] I. Sadli, P. Thounthong, J.-P. Martin, S. Raël, B. Davat, J. Power Sources 156 (2006) 119–125.